LETTER

doi:10.1038/nature25439

Atomic structure of the eukaryotic intramembrane RAS methyltransferase ICMT

Melinda M. Diver[1,2]†, Leanne Pedi[1], Akiko Koide[3,4], Shohei Koide[3,5] & Stephen B. Long[1]

The maturation of RAS GTPases and approximately 200 other cellular CAAX proteins involves three enzymatic steps: addition of a farnesyl or geranylgeranyl prenyl lipid to the cysteine (C) in the C-terminal CAAX motif, proteolytic cleavage of the AAX residues and methylation of the exposed prenylcysteine residue at its terminal carboxylate[1]. This final step is catalysed by isoprenylcysteine carboxyl methyltransferase (ICMT), a eukaryote-specific integral membrane enzyme that resides in the endoplasmic reticulum[2]. ICMT is the only cellular enzyme that is known to methylate prenylcysteine substrates; methylation is important for the biological functions of these substrates, such as the membrane localization and subsequent activity of RAS[1], prelamin A[3] and RAB[4]. Inhibition of ICMT has potential for combating progeria[3] and cancer[5–8]. Here we present an X-ray structure of ICMT, in complex with its cofactor, an ordered lipid molecule and a monobody inhibitor, at 2.3 Å resolution. The active site spans cytosolic and membrane-exposed regions, indicating distinct entry routes for the cytosolic methyl donor, S-adenosyl-L-methionine, and for prenylcysteine substrates, which are associated with the endoplasmic reticulum membrane. The structure suggests how ICMT overcomes the topographical challenge and unfavourable energetics of bringing two reactants that have different cellular localizations together in a membrane environment—a relatively uncharacterized but defining feature of many integral membrane enzymes.

ICMT from the beetle *Tribolium castaneum* exhibited superior biochemical stability in detergent-containing solutions in comparison to other orthologues and was used for biochemical characterization and structure determination (see Methods). Human and beetle ICMT share the same predicted topology[9] and have 58% amino acid sequence identity within the region thought to contain the active site[10] (amino acids 90–281; Extended Data Fig. 1). Beetle ICMT demonstrated robust methylation of prenylcysteine substrates both in cellular membranes and in the purified form, and exhibited kinetic parameters similar to those of human ICMT[11,12] (Extended Data Fig. 2). We engineered a synthetic ICMT-binding protein called a 'monobody', based on a randomized fibronectin protein domain, for use as a crystallization chaperone[13]. The monobody is an inhibitor of ICMT ($IC_{50} \approx 1\,\mu M$), and exhibits specificity for the beetle orthologue (Extended Data Fig. 2g, h). Crystals of purified ICMT–monobody complex were obtained in the lipidic-cubic phase[14] in the presence of the S-adenosyl-L-homocysteine (AdoHcy) cofactor and the prenylcysteine substrate N-acetyl-S-geranylgeranyl-L-cysteine (AGGC) (Extended Data Fig. 2a). Experimental phases yielded high-quality electron-density maps that enabled the placement of all amino acids of ICMT and the monobody (Extended Data Fig. 3a). The refined atomic coordinates have good stereochemistry and an R_{free} value of 24.6% (Extended Data Table 1).

ICMT contains eight transmembrane α-helices (M1–M8) and would reside almost entirely within the endoplasmic reticulum membrane in a cellular context (Fig. 1a, b). The largest cytosolic region of the enzyme, which protrudes approximately 12 Å away from the membrane and encompasses the binding site for AdoHcy, is formed by an extension of M8 together with a structurally ordered connection between M6 and M7 (the M6–M7 connector) plus a short 'cap' helix near the C terminus. The M6–M7 connector does not fully reach the luminal side, but is stabilized within the transmembrane region by interactions with the M5–M6 connector, which lies beneath it (Fig. 1b and Extended Data Fig. 4a). Additionally, the M5 helix would not span the bilayer. Its N terminus, capped by a hydrogen bond with Ser128, is positioned within the membrane region, about 10 Å from the cytosolic side (Fig. 1 and Extended Data Fig. 5b). Unusually, the M4 and M5 helices are connected by a 25 Å-long extended segment (Pro115–Pro129) that traverses diagonally in the membrane-spanning region (Fig. 1c and Extended Data Fig. 5a). The M1–M3 region, which is unique to ICMT enzymes from animals (Extended Data Fig. 1), makes extensive contacts with M4 and the M4–M5 connector. Helices M1, M2 and M3 associate with one another and are stabilized, in part, by GXXXG-like helical packing motifs between M1 and M3[15] (Extended Data Fig. 6a). The non-covalent association is strong enough that M1 and M2 remain associated with the core of the enzyme following proteolytic cleavage of the M2–M3 loop (Extended Data Fig. 6). Congruently, genetic deletion of M1 and M2 renders human ICMT inactive[12].

The structure provides context for a large body of functional data on ICMT[9–12,16]. Residues that disrupt catalytic activity when mutated define the active site on the structure (Fig. 2a), the location of which had remained elusive owing to the broad distribution of these residues in the primary structure (Extended Data Fig. 1). In the cell, the active site would be located mostly within the cytosolic leaflet of the membrane, and is contained between M4 and the C terminus in the primary structure (Fig. 2a). AdoHcy is encapsulated within a pocket that secludes it from both the aqueous environment of the cytosol and the lipid membrane, and is formed by the M6–M7 connector, the cytosolic extension of M8 and the cap helix (Fig. 2b, c). The release of AdoHcy and the subsequent binding of S-adenosyl-L-methionine (AdoMet) could occur via hinged displacement of the M6–M7 connector towards the cytosol, in which there is a reservoir of micromolar concentrations of AdoMet; Gly181 and Ser193 are potential hinge points for this mechanism (Fig. 2c). The perfectly conserved residues Phe184, Tyr204 and Glu250 appear to be particularly important for positioning AdoHcy through direct contacts (Fig. 2c), and completely abolish activity when mutated to alanine[12,16] (Extended Data Fig. 1). The active site could accommodate the methyl group of AdoMet in a slender 'tunnel' (Fig. 2b and Extended Data Fig. 4c), suggesting that the observed conformation of AdoHcy is analogous to the conformation when the methyl donor is bound.

ICMT accommodates a breadth of protein substrates. This includes all prenylated (farnesylated and geranylgeranylated) and proteolytically

[1]Structural Biology Program, Memorial Sloan Kettering Cancer Center, 1275 York Avenue, New York, New York 10065, USA. [2]Graduate Program in Biochemistry and Structural Biology, Cell and Developmental Biology, and Molecular Biology, Weill Cornell Medicine Graduate School of Medical Sciences, 1300 York Avenue, New York, New York 10065, USA. [3]Perlmutter Cancer Center, New York University Langone Medical Center, 430 East 29th Street, New York, New York 10016, USA. [4]Department of Medicine, New York University Langone Medical Center, 430 East 29th Street, New York, New York 10016, USA. [5]Department of Biochemistry and Molecular Pharmacology, New York University Langone Medical Center, 430 East 29th Street, New York, New York 10016, USA. †Present address: Department of Physiology, University of California, San Francisco, San Francisco, California 94158, USA.

© 2018 Macmillan Publishers Limited, part of Springer Nature. All rights reserved.

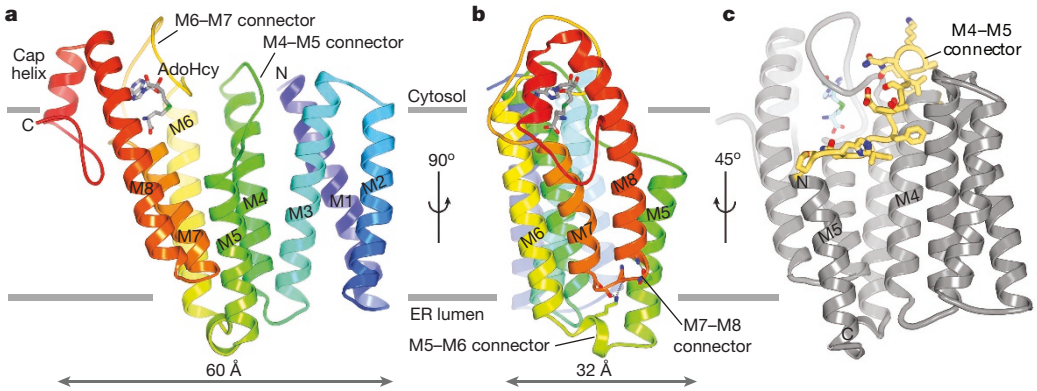

Figure 1 | Architecture of ICMT. a, Ribbon representation with secondary structure elements coloured blue-to-red from N terminus to C terminus. Horizontal lines indicate approximate boundaries of the endoplasmic reticulum (ER) membrane. **b**, Orthogonal view, showing interactions between the M5–M6 and M7–M8 connectors (sticks with hydrogen bonds drawn as dashed lines). **c**, View highlighting the location of the M4–M5 connector (yellow with drawn side chains).

processed CAAX proteins, as well certain RAB GTPases that have two geranylgeranyl groups attached to the cysteine residues of their C-terminal CXC motif[1]. The structure suggests that the prenyl moiety of the substrate binds in a deep cavity within the active site that extends from the cofactor pocket into the transmembrane region (Figs 2b and 3a). This cavity is approximately 22 Å long and 6 Å wide, and is formed by regions of the M4, M5, M7 and M8 helices. Approximately two thirds of the cavity would be exposed to the cytosolic leaflet of the lipid bilayer via a lateral crevice between helices M5 and M8 (Figs 2b and 3b). A tube of electron density consistent with a lipid is present in the cavity (Fig. 3a). Although the 20-carbon geranylgeranyl group of the AGGC substrate that was present during crystallization could account for the density, we cannot be sure of its identity, and therefore modelled a monoolein lipid into the density (Fig. 3a and Extended Data Fig. 3b). The cavity would also accommodate the 15-carbon farnesyl group. Similar to the binding site for the prenyl group in water-soluble enzymes such as farnesyltransferase[17], the proposed prenyl-binding cavity is lined primarily by aromatic amino acids (Tyr95, Met99, Phe102, Val124, Asn126, Tyr131, Trp215, Trp218, Tyr235, Phe242 and Phe243) that markedly reduce enzyme activity when mutated[12] (Extended Data Fig. 1). For doubly geranylgeranylated CXC proteins, the second prenyl group could be accommodated in the crevice between M5 and M8 and/or in the adjacent membrane while the C-terminal geranylgeranyl group occupies the active site.

The structure of a methyltransferase from the prokaryotic organism *Methanosarcina acetivorans,* which we refer to as *Ma*MTase, highlights the diversity within the integral membrane methyltransferase family[16] (Extended Data Fig. 7). Despite sharing only 14% sequence identity with ICMT, *Ma*MTase was previously referred to as *Ma*-ICMT, but this nomenclature was misleading because its biological substrates are unknown, it cannot methylate prenylated-peptide substrates[16] and there are no known prenylated proteins in prokaryotes. Nevertheless, the binding sites for AdoHcy are analogous in ICMT and *Ma*MTase (Extended Data Fig. 7) and the cofactor-binding domain of ICMT, which spans from M6 through the cap helix, shares a recognizable fold not only with regions of *Ma*MTase, but also with regions of a prokaryotic integral membrane sterol reductase that utilizes a nicotinamide adenine dinucleotide phosphate ($NADP^+$) cofactor[16,18]; this suggests that this domain represents a structural motif for soluble cofactor binding to integral membrane enzymes (Extended Data Fig. 8). Other regions of the active site of ICMT show minimal similarity to *Ma*MTase; the substrate-binding sites differ in size, amino acid composition and membrane exposure (Fig. 3b, Extended Data Figs 7a and 8).

The monobody inhibitor binds ICMT adjacent to the active site and interacts with portions of M5, M8 and the M6–M7 loop (Fig. 3c). The 'FG loop' of the monobody, which is diversified in the combinatorial library[13], dips into the membrane region and presents a tryptophan residue (Trp80) that occupies part of the crevice between M5 and M8 (Fig. 3d). It also contacts a portion of the modelled lipid. Although monobodies typically recognize native surfaces of their cognate proteins[19], to evaluate whether the structure of ICMT was affected

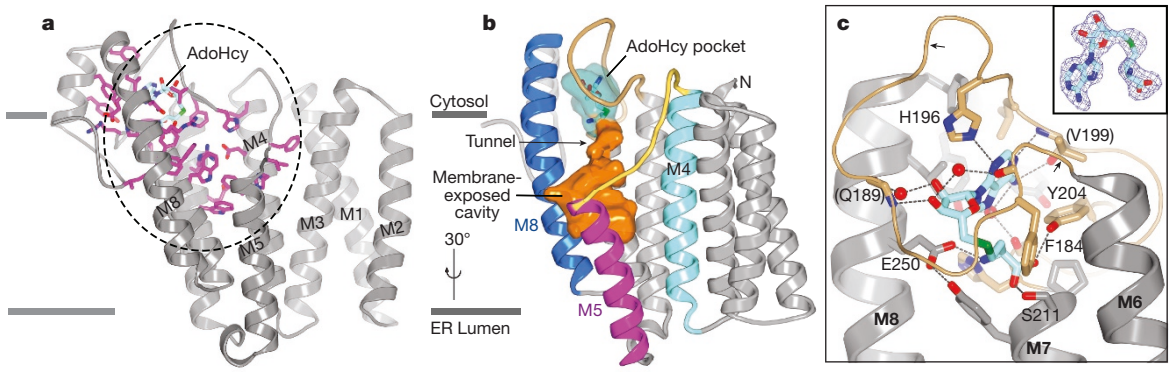

Figure 2 | The active site. a, Three-dimensional clustering of key residues identifies the active site. Residues that diminish specific activity by more than 95% when mutated[12] (Extended Data Fig. 1) are drawn in magenta on a ribbon representation. The high concentration of such residues within the dashed region demarcates the active site. **b**, The active site, depicted as a molecular surface within the ribbon representation. The AdoHcy pocket is cyan; the membrane-exposed cavity is orange. **c**, Interactions with AdoHcy (sticks with cyan carbon atoms). Dashed lines indicate hydrogen bonds. Water molecules are shown as red spheres. Nitrogen, blue; oxygen, red; and sulfur, green. The M6–M7 connector is tan. Arrows mark the locations of Gly181 and Ser193; parentheses indicate hydrogen bonds with backbone atoms. Inset shows electron density for AdoHcy (simulated annealing omit F_o–F_c map, contoured at 3σ).

© 2018 Macmillan Publishers Limited, part of Springer Nature. All rights reserved.

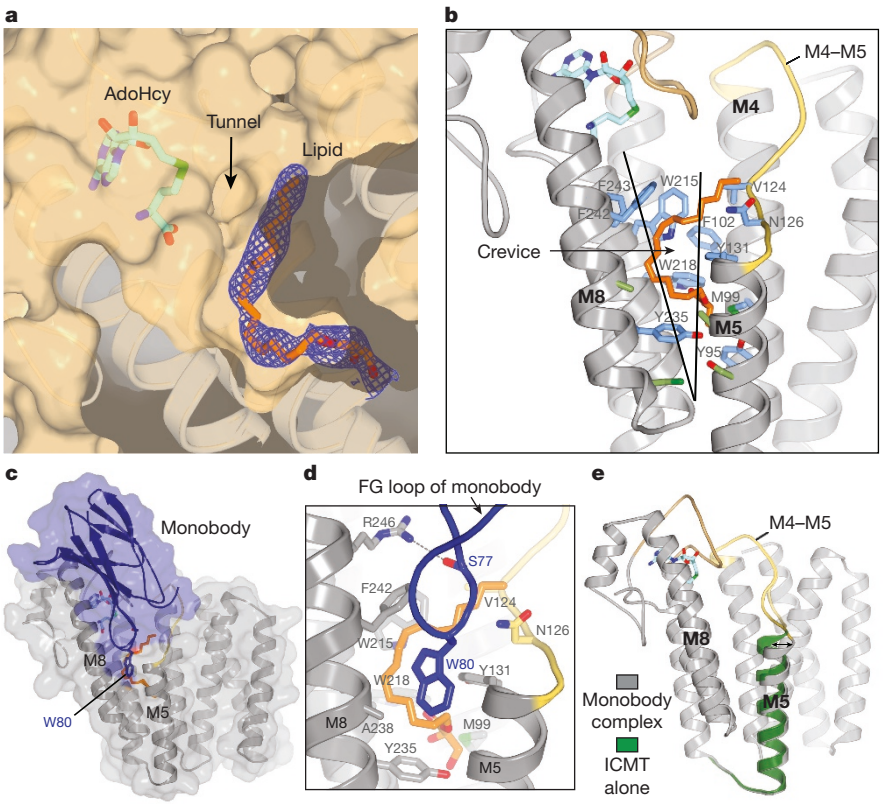

Figure 3 | Lipid-binding cavity and monobody complex. a, The active-site cavity containing a lipid molecule. Electron density (blue mesh, $2F_o–F_c$ map contoured at 1σ) for a monoolein lipid (orange sticks) is shown on a cutaway view of the molecular surface (tan). The tunnel between AdoHcy (sticks) and the lipid-binding cavity is indicated. Helices below the surface are depicted as ribbons. **b**, The crevice and amino acids comprising the lipid-binding cavity. A portion of ICMT is depicted as ribbons with the M4–M5 connector in yellow and the M6–M7 connector in tan. The crevice between M5 and M8 is indicated by a wedge. Amino acids within van der Waals distances of the lipid are coloured blue; those that line the crevice are green. **c**, Monobody complex. A semi-transparent representation of the molecular surface of the complex (ICMT, grey; monobody, blue) is shown surrounding ribbon representations. **d**, Close view of the FG loop of the monobody (blue) interacting with ICMT (predominately grey). Trp80 and Ser77 of the monobody are shown as sticks. A hydrogen bond between Ser77 and Arg246 of ICMT is shown as a dashed line. The monoolein molecule (orange) and ICMT residues surrounding it are shown as sticks. **e**, Comparison of structures with and without the monobody (coloured as indicated). An arrow highlights the tilting of M5; the overall structures are otherwise indistinguishable.

by the monobody, we determined a 4.0 Å resolution X-ray structure of ICMT without the monobody (Methods). The only discernable difference is a slight (around 5°) tilting of M5, which could also be due to crystallization in detergent rather than lipidic cubic phase and/or a degree of inherent flexibility (Fig. 3e and Extended Data Fig. 3e; the overall r.m.s.d. for Cα atoms is 0.5 Å). The lengthy lipid-binding cavity and the crevice between M5 and M8 leading to it, hallmark features of the active site, are present without the monobody. The location of the monobody suggests that it would prevent prenylated substrates from reaching the active site and/or block product release. Hydrogen bonding between Ser77 of the monobody and Arg246 of ICMT may also contribute to its inhibitory function (Fig. 3d), as we predict that Arg246 coordinates the C-terminal carboxylate of the prenylcysteine. Although specific contacts between ICMT and cognate protein substrates are expected to be confined to their prenylcysteine moieties[20–22], the positioning of the monobody adjacent to the active site and on the cytosolic side above the crevice between M5 and M8 may demarcate the approximate location of a protein substrate as its C-terminal prenylcysteine undergoes methylation (Figs 3c and 4a). Hydrophobic molecules that bind in the crevice would be expected to inhibit the enzyme; this may be the mode of action of some existing ICMT inhibitors.

The protein substrates of ICMT are amphipathic; their prenyl group or groups partition into the endoplasmic reticulum membrane[1], and their C-terminal carboxylate and variable protein portions are hydrophilic and exposed to the cytosol. The crevice between M5 and M8, which would be accessible to the hydrophobic core of the membrane and leads directly to the active site, provides a plausible route for prenyl entry by lateral diffusion (Fig. 4a). The positions of the N-terminal end of M5 and the M4–M5 connector create a hydrophilic depression within the membrane-embedded region of ICMT, and might induce a concomitant depression in the proximal lipids of the bilayer (Extended Data Figs 3c and 9) that would accommodate the upstream peptide, as has been modelled for KRAS4B (Fig. 4a). Suggestive of an important role, the M4–M5 connector is highly conserved and greatly diminishes catalytic activity when mutated[12] (Fig. 2a and Extended Data Fig. 1). Hydrophobic residues (Phe123, Val124 and Leu125) presumably anchor it in the membrane, and hydrophilic residues (Asn126, His127 and Ser128) give it amphipathic character (Extended Data Fig. 5a). The enzyme appears to achieve substrate specificity by the distinct position, shape, proportion and amphiphilicity of its active site.

We constructed a model of a transition state based on the structure of ICMT (Fig. 4b). The negatively charged carboxylate of the prenylcysteine substrate, the nucleophile in the direct-transfer mechanism, is coordinated and positioned for catalysis by two arginine residues, Arg173 (on M6) and Arg246 (on M8), which also provide specificity for the carboxylate. In the X-ray structure, Arg173 and Arg246 are stabilized by hydrogen-bonding networks and two water molecules occupy the proposed location of the carboxylate (Extended Data Fig. 4b). Similar to other methyltransferases that use AdoMet as the methyl donor[23], and supported by mutagenesis data[12] (Extended Data Fig. 1), we predict that the methyl group of AdoMet makes three unconventional hydrogen bonds involving carbon as the hydrogen-bond donor that help stabilize the transition state (Fig. 4b).

© 2018 Macmillan Publishers Limited, part of Springer Nature. All rights reserved.

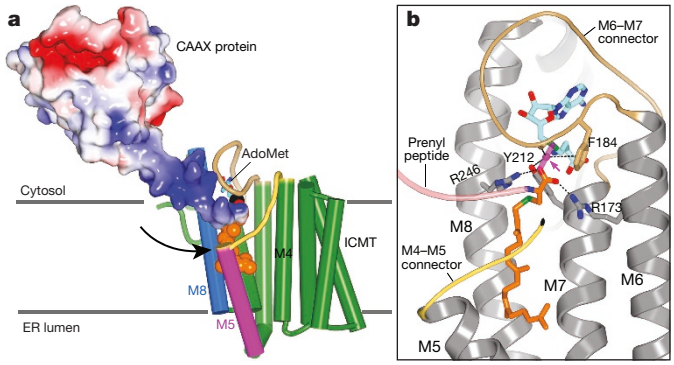

Figure 4 | Substrate access and transition-state models. a, Substrate access in a hypothetical ternary complex. ICMT is depicted with cylindrical helices; AdoMet is modelled from AdoHcy. The binding of an ICMT substrate, in this case partially processed KRAS4B (coloured molecular surface; RCSB Protein Data Bank (PDB) ID: 5TAR) with attached geranylgeranyl group (orange spheres), is shown. An arrow denotes a plausible path for membrane-partitioned substrates to reach the active site through the crevice between M5 and M8. The hypervariable region of the substrate upstream of the CAAX motif is dark blue, indicating its basic character in KRAS4B. **b**, Transition-state model. Translucent magenta sticks depict the scissile and nascent bonds, with the methyl group of AdoMet (cyan carbons) shown as a magenta sphere (indicated by the arrow). The C-terminal carboxylate of the prenylcysteine substrate (orange carbons) forms hydrogen bonds (dashes) with Arg173 and Arg246 that orient it for inline nucleophilic attack. The transition state is further stabilized by interactions (dashes) with the methyl group being transferred: a CH–O hydrogen bond with the side chain hydroxyl of Tyr212, a CH–O hydrogen bond with the backbone carbonyl oxygen of Asn185, and a CH–π interaction with the aromatic face of Phe184. All of the amino acid side chains proposed to be involved in transition state stabilization are perfectly conserved among ICMT enzymes. In the figure, the peptide portion of a hypothetical substrate is drawn as a pink ribbon, a portion of the M4–M5 connector is coloured yellow, and the enzyme is shown as grey ribbons; M1–M4 are removed for clarity.

A recent study indicates that human *ICMT* has a synthetic lethal interaction with oncogenic *RAS*[8], suggesting that ICMT inhibitors could be effective against RAS-driven cancers. ICMT inhibitors may also be useful for treating progeria, the pathology of which is attributed to the accumulation of a prenylated and methylated form of prelamin A at the nuclear envelope[3,24]. This structure of ICMT will contribute toward efforts to develop inhibitors. More generally, our study describes the atomic structure of an intramembrane enzyme, a class of proteins for which a relatively small number of structures have been determined. Many enzymes that are embedded in biological membranes facilitate the access of reactants that have drastically different physiochemical properties to a common active site and maintain them in close proximity for catalysis. The structure provides insight into how one enzyme accomplishes these complex tasks while maintaining specificity for its diverse substrates.

Online Content Methods, along with any additional Extended Data display items and Source Data, are available in the online version of the paper; references unique to these sections appear only in the online paper.

Received 5 September; accepted 7 December 2017.
Published online 17 January 2018.

1. Wang, M. & Casey, P. J. Protein prenylation: unique fats make their mark on biology. *Nat. Rev. Mol. Cell Biol.* **17,** 110–122 (2016).
2. Dai, Q. *et al.* Mammalian prenylcysteine carboxyl methyltransferase is in the endoplasmic reticulum. *J. Biol. Chem.* **273,** 15030–15034 (1998).
3. Ibrahim, M. X. *et al.* Targeting isoprenylcysteine methylation ameliorates disease in a mouse model of progeria. *Science* **340,** 1330–1333 (2013).
4. Court, H., Ahearn, I. M., Amoyel, M., Bach, E. A. & Philips, M. R. Regulation of NOTCH signaling by RAB7 and RAB8 requires carboxyl methylation by ICMT. *J. Cell Biol.* **216,** 4165–4182 (2017).
5. Berndt, N., Hamilton, A. D. & Sebti, S. M. Targeting protein prenylation for cancer therapy. *Nat. Rev. Cancer* **11,** 775–791 (2011).
6. Cox, A. D., Fesik, S. W., Kimmelman, A. C., Luo, J. & Der, C. J. Drugging the undruggable RAS: Mission possible? *Nat. Rev. Drug Discov.* **13,** 828–851 (2014).
7. Lau, H. Y., Tang, J., Casey, P. J. & Wang, M. Isoprenylcysteine carboxylmethyltransferase is critical for malignant transformation and tumor maintenance by all RAS isoforms. *Oncogene* **36,** 3934–3942 (2017).
8. Wang, T. *et al.* Gene essentiality profiling reveals gene networks and synthetic lethal interactions with oncogenic RAS. *Cell* **168,** 890–903.e15 (2017).
9. Wright, L. P. *et al.* Topology of mammalian isoprenylcysteine carboxyl methyltransferase determined in live cells with a fluorescent probe. *Mol. Cell. Biol.* **29,** 1826–1833 (2009).
10. Romano, J. D. & Michaelis, S. Topological and mutational analysis of *Saccharomyces cerevisiae* Ste14p, founding member of the isoprenylcysteine carboxyl methyltransferase family. *Mol. Biol. Cell* **12,** 1957–1971 (2001).
11. Baron, R. A. & Casey, P. J. Analysis of the kinetic mechanism of recombinant human isoprenylcysteine carboxylmethyltransferase (ICMT). *BMC Biochem.* **5,** 19 (2004).
12. Diver, M. M. & Long, S. B. Mutational analysis of the integral membrane methyltransferase isoprenylcysteine carboxyl methyltransferase (ICMT) reveals potential substrate binding sites. *J. Biol. Chem.* **289,** 26007–26020 (2014).
13. Koide, A., Wojcik, J., Gilbreth, R. N., Hoey, R. J. & Koide, S. Teaching an old scaffold new tricks: monobodies constructed using alternative surfaces of the FN3 scaffold. *J. Mol. Biol.* **415,** 393–405 (2012).
14. Caffrey, M. & Cherezov, V. Crystallizing membrane proteins using lipidic mesophases. *Nat. Protoc.* **4,** 706–731 (2009).
15. Lemmon, M. A., Treutlein, H. R., Adams, P. D., Brünger, A. T. & Engelman, D. M. A dimerization motif for transmembrane alpha-helices. *Nat. Struct. Biol.* **1,** 157–163 (1994).
16. Yang, J. *et al.* Mechanism of isoprenylcysteine carboxyl methylation from the crystal structure of the integral membrane methyltransferase ICMT. *Mol. Cell* **44,** 997–1004 (2011).
17. Long, S. B., Casey, P. J. & Beese, L. S. Reaction path of protein farnesyltransferase at atomic resolution. *Nature* **419,** 645–650 (2002).
18. Li, X., Roberti, R. & Blobel, G. Structure of an integral membrane sterol reductase from *Methylomicrobium alcaliphilum*. *Nature* **517,** 104–107 (2015).
19. Koide, S. Engineering of recombinant crystallization chaperones. *Curr. Opin. Struct. Biol.* **19,** 449–457 (2009).
20. Tan, E. W., Pérez-Sala, D., Cañada, F. J. & Rando, R. R. Identifying the recognition unit for G protein methylation. *J. Biol. Chem.* **266,** 10719–10722 (1991).
21. Pérez-Sala, D., Gilbert, B. A., Tan, E. W. & Rando, R. R. Prenylated protein methyltransferases do not distinguish between farnesylated and geranylgeranylated substrates. *Biochem. J.* **284,** 835–840 (1992).
22. Anderson, J. L., Henriksen, B. S., Gibbs, R. A. & Hrycyna, C. A. The isoprenoid substrate specificity of isoprenylcysteine carboxylmethyltransferase: development of novel inhibitors. *J. Biol. Chem.* **280,** 29454–29461 (2005).
23. Horowitz, S. *et al.* Conservation and functional importance of carbon-oxygen hydrogen bonding in AdoMet-dependent methyltransferases. *J. Am. Chem. Soc.* **135,** 15536–15548 (2013).
24. Gordon, L. B., Rothman, F. G., López-Otín, C. & Misteli, T. Progeria: a paradigm for translational medicine. *Cell* **156,** 400–407 (2014).

Supplementary Information is available in the online version of the paper.

Acknowledgements We thank D. Julius, C. D. Lima, M. Luo, N. P. Pavletich, R. K. Hite, S. Shuman and members of the Long laboratory for discussions. Beamlines 24-ID and 23-ID at the Advanced Photon Source are supported by NIH grants ACB-12002, AGM-12006, P41 GM103403 and S10 RR029205, under DOE contract DE-AC02-06CH11357. This work was supported, in part, by an American Heart Association Pre-doctoral Fellowship (M.M.D.), a Burroughs Wellcome Career Award (S.B.L), the Geoffrey Beene Cancer Research Center at MSKCC (S.B.L.), a core-facilities support grant to MSKCC (P30 CA008748) and NIH grant U54-GM087519 (S.K.).

Author Contributions M.M.D. and L.P. cloned, expressed and purified proteins. A.K. and S.K. developed monobodies. M.M.D. performed all other experiments. M.M.D. and S.B.L. designed experiments, determined structures, analysed results and prepared the manuscript with contributions from all authors.

Author Information Reprints and permissions information is available at www.nature.com/reprints. The authors declare no competing financial interests. Readers are welcome to comment on the online version of the paper. Publisher's note: Springer Nature remains neutral with regard to jurisdictional claims in published maps and institutional affiliations. Correspondence and requests for materials should be addressed to S.B.L. (Longs@mskcc.org).

Reviewer Information *Nature* thanks M. Bergö, P. Casey and O. Nureki for their contribution to the peer review of this work.

© 2018 Macmillan Publishers Limited, part of Springer Nature. All rights reserved.

METHODS

Cloning, expression, and purification of ICMT. *T. castaneum* (beetle) ICMT (UniProt accession D6WJ77) was selected as a candidate for protein purification and crystallization trials from among 76 eukaryotic ICMT orthologues that were evaluated using the fluorescence-detection size-exclusion chromatography (FSEC) pre-crystallization screening technique[12,25]. The cDNA (synthesized by Bio Basic) was ligated into the EcoRI and SalI restriction sites of the *Pichia pastoris* expression vector pPICZ-C (Invitrogen Life Technologies) and encodes the full-length protein followed by a C-terminal antibody-affinity tag (Ala-Ala-Glu-Gly-Glu-Glu-Phe) that is recognized by the anti-tubulin antibody YL1/2[26]. For the crystals of ICMT alone, two point mutations of surface residues were introduced to improve crystallizability (G151A and E154A). Transformation into *P. pastoris*, expression and cryo-lysis were performed as previously described[27].

Lysed cells (40 g) were re-suspended in 200 ml of buffer containing 10 mM Tris-HCl, pH 7.5, 150 mM KCl, 2 mM tri(2-carboxyethyl)phosphine (TCEP, Soltec Ventures; a 275 mM stock solution of TCEP was prepared in 1 M KOH to yield pH ~7.5), 2 mM $CaCl_2$, 25 μM AdoHcy, 0.15 mg/ml DNase I (Sigma-Aldrich), 1:1,000 dilution of Protease Inhibitor Cocktail Set III (EDTA free, CalBiochem), 1 mM benzamidine (Sigma-Aldrich), 0.5 mM 4-(2-aminoethyl) benzenesulfonyl fluoride hydrochloride (AEBSF, Gold Biotechnology) and 1:1,000 dilution of aprotinin (Sigma-Aldrich). Cell lysate was adjusted to pH 7.5 using 1 M KOH, 2 g decyl maltose neopentyl glycol (DMNG, Anatrace) was added to the cell lysate and the mixture was stirred at room temperature for 45 min to extract ICMT from the membranes. The sample was then centrifuged at 43,000*g* for 40 min at 12 °C and the supernatant was filtered through a 0.22-μm polystyrene membrane (Millipore). YL1/2 antibody (IgG, expressed from hybridoma cells and purified by ion-exchange chromatography using standard methods) was coupled to CNBr-activated sepharose beads (GE Healthcare) according to the manufacturer's protocol. Approximately 0.4 ml of YL1/2 antibody beads were added to the sample for each 1 g of *P. pastoris* cells and the mixture was rotated at room temperature for 1 h. Beads were collected on a column, washed with four column volumes of buffer containing 10 mM Tris-HCl, pH 7.5, 150 mM KCl, 2 mM TCEP, 2 mM $CaCl_2$, 25 μM AdoHcy and 1 mM DMNG, and the protein was eluted with buffer containing 100 mM Tris-HCl, pH 7.5, 150 mM KCl, 2 mM TCEP, 2 mM $CaCl_2$, 25 μM AdoHcy, 1 mM DMNG and 5 mM Asp–Phe peptide (Sigma-Aldrich) or Glu–Glu–Phe peptide (Peptide 2.0).

ICMT–monobody co-crystallization in lipidic cubic phase. Following elution from the antibody-affinity column, the protein was combined with the monobody (designated MB-15) in a 1:3 molar ratio (ICMT:monobody). The mixture was concentrated to 500 μl using a 30-kDa concentrator (Amicon Ultra, Millipore) and the ICMT–monobody complex was purified using a Superdex 200 Increase size-exclusion column (GE Healthcare) in 10 mM Tris-HCl, pH 7.5, 150 mM KCl, 5 mM TCEP, 2 mM $CaCl_2$, 25 μM AdoHcy and 0.2 mM DMNG. The fractions corresponding to the ICMT–monobody complex and the free monobody were combined (to ensure an excess of monobody), 500 μM AdoHcy was added, and the sample was concentrated to ~10 mg/ml using a 100-kDa Vivaspin-2 concentrator (Satorius Stedim Biotech). Some of the excess monobody passed through the concentrator. Following concentration, 1 mM N-acetyl-S-geranylgeranyl-L-cysteine (AGGC, from a 100 mM stock in DMSO, Enzo Life Sciences) was added before crystallization.

The ICMT–monobody complex was combined with a mixture of 9.9 monoacylglycerol (monoolein, Nu-Chek Prep) at a ratio of 40:60 (v:v, ICMT:monoolein) using a manual syringe mixer at 20 °C following an established protocol[14]. A Gryphon LCP robot (Art Robbins Instruments) was used to dispense 50-nl mesophase drops onto 96-well glass sandwich plates (Marienfeld). The LCP boluses were overlaid with 800 nl precipitant solution. Drops were sealed with a glass coverslip, incubated at 20 °C and imaged periodically using a RockImager (Formulatrix). The precipitant solution for the best crystal consisted of 30% PEG 400, 100 mM NaCl and 100 mM Na HEPES, pH 7.5. Crystals also grew in other salts, including 100 mM $LiSO_4$ and 100 mM $AmSO_4$. Crystals appeared after one day and reached approximately 30–60 μm in size within two to three days. To collect the LCP crystals, the glass coverslip was scored using a glass cutter, the LCP bolus was overlaid with ~2 μl of additional precipitant solution, and the crystals were collected using MiTeGen MicroMounts and submerged in liquid nitrogen.

Crystallization in detergent. ICMT was purified as described above except that 1 mg/ml total brain lipids (Avanti) was added to the purification buffers. The elution from the antibody affinity column was concentrated to 500 μl using a 50-kDa concentrator (Amicon Ultra, Millipore) and applied to a Superdex 200 Increase size-exclusion column (GE Healthcare) that was equilibrated in 10 mM Tris-HCl, pH 7.5, 150 mM KCl, 5 mM TCEP, 2 mM $CaCl_2$, 25 μM AdoHcy, 1 mM DMNG and 0.02 mg/ml total brain lipids. Fractions containing ICMT were pooled, supplemented with 500 μM AdoHcy, and concentrated to 5–10 mg/ml using a 50 kDa concentrator (Vivaspin-2; Sartorius). ICMT crystals were obtained by vapour diffusion using 300 nl ICMT and 300 nl crystallization solution and a Mosquito crystallization robot (TTP Labtech) over reservoirs containing 100 μl precipitant solution. The crystals were obtained from 24–28% PEG400 (v/v), 200 mM $CaCl_2$ or 200 mM $MgCl_2$, 50 mM Na acetate, pH 5.0–6.5, at 4 °C and reached a size of approximately 100–400 μm within two to three weeks. The crystals were then transferred through a series of five steps using the components of an equilibrated drop to increase the PEG 400 concentration to 35% before flash-cooling in liquid nitrogen.

Monobody generation. General methods for phage- and yeast-display library sorting and gene shuffling have been described[13,28]. His_{10}-tagged beetle ICMT protein, purified from *P. pastoris* and solubilized in 10 mM Tris-HCl, pH 7.5, 150 mM NaCl, 25 μM AdoHcy, 50 μM AGGC and 1 mM DMNG, was mixed with an equimolar concentration of BTtrisNTA, a high-affinity His-tag ligand conjugated with biotin[29], so as to capture the target proteins with streptavidin magnetic beads in phage-display selection and to detect them with fluorescent dye-labelled streptavidin in yeast-surface-display experiments[30]. Two separate monobody libraries, denoted 'loop' and 'side', were used to generate monobodies with diverse binding-surface topography[13]. Four rounds of phage-display library sorting were performed using target concentrations of 100, 100, 100 and 50 nM for the first, second, third and fourth rounds, respectively, at room temperature. Three rounds of yeast display library sorting were performed, using a fluorescence-activated cell sorter (FACSAria, BD Biosciences). The first round was to enrich clones that did not bind to 500 nM BTtrisNTA but without ICMT (negative sorting), and the second and third rounds were to enrich clones that bound to 500 nM and 250 nM ICMT–BTtrisNTA complex (positive sorting). Target binding of individual clones was tested using yeast display and three were selected for purification. The monobody proteins were expressed in *Escherichia coli* using the expression vector pHBT, which adds an N-terminal His_6 tag followed by a biotin-acceptor tag and a TEV-cleavage site[31]. Co-crystallization with one of these monobodies (designated MB-15) yielded crystals with good diffraction. For purification of MB-15, frozen cells were mechanically lysed in a mixer mill (Retsch model PM 100; 8 × 3 min at 400 r.p.m.) using steel balls. Lysed cells (6 g) were re-suspended in 50 ml buffer containing 50 mM Tris-HCl, pH 8.0, 500 mM NaCl, 0.2 mg/ml DNase I and 200 μM AEBSF. The mixture was stirred at 4 °C for 30 min. The sample was then centrifuged at 43,000*g* for 30 min at 4 °C and the supernatant was filtered through a 0.22-μm polystyrene membrane (Millipore). The supernatant was applied to a column containing 4 ml immobilized metal-affinity chromatography resin charged with cobalt (TALON, BD Biosciences), the resin was washed with 7.5 column volumes of buffer containing 20 mM Tris, pH 8.0 and 500 mM NaCl, and the protein was eluted with buffer containing 20 mM Tris, pH 8.0, 500 mM NaCl and 300 mM imidazole, pH 8.0. Following elution, 5 mM EDTA (pH 8.0) was added and the samples were centrifuged (43,000*g*, 10 min, 17 °C) to pellet any precipitated protein. The N-terminal affinity tag was removed by treatment with TEV protease (4 °C; 1:20, wt:wt, TEV:monobody) for 16 h and an additional 8 h with a 1:40 ratio of TEV:monobody). The amino sequence of MB-15 is: MKHHHHHHSSGLNDIFEAQKIEWHEENLYFQGSVSSVPTKLEVVAATPTSLLISWDAPAVTVDLYVITYGETGGNSPVQEFKVPGSKSTATISGLKPGVDYTITVYAFSSYYWPSYKGSPISINYRT. The underlined portion indicates the peptide removed by TEV cleavage. Purified MB-15 was stored at −80 °C until use.

Structure determination. X-ray data were collected at beamlines 23ID-D and 24ID-C of the Advanced Photon Source (APS, Argonne). Diffraction data were collected using an oscillation angle of 0.3° and high redundancy was obtained by collecting data from multiple locations throughout the crystals. For phasing of the ICMT–monobody complex, Se–Met labelled ICMT protein was generated by producing the enzyme in High Five insect cells (Invitrogen) using a baculovirus system with standard techniques. Diffraction data were processed using the HKL3000 suite[32]. The crystals diffracted X-rays to 2.3 Å resolution and each asymmetric unit contained one ICMT–monobody complex. Initial experimental phases (35–4 Å) for the ICMT–monobody complex (space group $P2_12_12_1$) were determined using the SIRAS phasing method in SHARP and improved using solvent flattening[33]. Five Se–Met sites were located; they correspond to the five methionine residues of ICMT. Electron density for the monobody was discontinuous in these maps. The monobody was placed in the asymmetric unit using molecular replacement (using an ensemble of monobody structures, PDB ID: 3UYO, 1FNA, 2QBW and 2OCF, and a homology model of MB-15 based on PDB ID: 3UYO) in Phaser[34]. At this point, well-defined electron density was observed for the entire complex. The atomic model was constructed using Coot and improved through iterative cycles of refinement using CNS and PHENIX[35–37]. Model validation was performed with MolProbity[38]. Each unit cell contains one ICMT–monobody complex. Data collection, phasing, and refinement statistics are shown in Extended Data Table 1.

The structure of ICMT in the absence of the monobody (space group $C222_1$) was determined by molecular replacement using the refined 2.3 Å resolution structure of ICMT from the monobody complex as a search model in Phaser[34].

© 2018 Macmillan Publishers Limited, part of Springer Nature. All rights reserved.

X-ray diffraction from the crystal of ICMT without monobody was anisotropic and the dataset was truncated to 4.2 Å resolution along b* using the Diffraction Anisotropy Server[39]. The electron density maps from Phaser showed continuous electron density throughout the model and indicated slight tilting of M5. The model was adjusted accordingly in Coot and refined in Phenix[36,37]. A composite simulated-annealing omit-electron density map was constructed using Phenix[36] and this map confirmed that the only discernable difference in the overall structure was the tilting of M5 (Fig. 3e and Extended Data Fig. 3e). Molecular graphics figures were prepared using PyMOL (http://www.pymol.org).

Enzymatic assay. The catalytic activity of ICMT was measured using a previously described assay, with slight modifications, to monitor [^{3}H]methyl incorporation into biotin-S-farnesyl-L-cysteine (BFC)[11,12]. For these assays, ICMT was either purified (as described above; using 0.2 mM DMNG detergent) or present as a GFP-fusion protein in HEK293-cell lysate[12] (GFP was fused to the N terminus and an AAEGEEF tag was present on the C terminus). For experiments using GFP-tagged ICMT, the preparation of the cell lysate and the determination of the ICMT concentration from the GFP fluorescence were as previously described[12]. The enzyme, either as purified ICMT in DMNG detergent or as GFP–ICMT in HEK293-cell lysate, was diluted into reaction buffer containing 150 mM NaCl, 5 mM $MgCl_2$, 1mM DTT and 100 mM HEPES pH 7.4 to yield an ICMT protein concentration of approximately 10 nM. For experiments using purified protein, the reaction buffer was supplemented with 10 μM DMNG. For the initial velocity curves, the data were fitted using GraphPad Prism 7 software as previously described[12]. For experiments used to study the effect of the monobody on activity (Extended Data Fig. 2f, g), enzymatic assays were performed with varying concentrations of monobody, a fixed amount (~10 nM) of enzyme, 5 μM BFC and 4 μM AdoMet, using either purified beetle ICMT or one of the following GFP-tagged ICMT orthologues in HEK293 cell lysate: beetle ICMT, human ICMT or *Anopheles gambiae* ICMT[12].

For initial velocity curves, the data were fitted to the following models using least-squares nonlinear regression with GraphPad Prism 7 software: (1) for the initial velocity versus AdoMet concentration curves, a Michaelis–Menten model was used, $Y = V_{max}X/(K_m + X)$; (2) for the initial velocity versus BFC concentration curves when substrate inhibition was not observed, an allosteric-sigmoidal model was used, $Y = V_{max}X^h/({K_{half}}^h + X^h)$; and (3) for the initial velocity versus BFC concentration curves when substrate inhibition was observed, an allosteric-sigmoidal model that takes into account substrate inhibition was used, $Y = V_{max}X^h/({K_{half}}^h + X^h(1 + X^h/{K_i}^h))$. In these equations Y is the initial velocity, X is the substrate concentration, h is the Hill coefficient, V_{max} is the maximum enzyme velocity, K_{half} and K_m are the concentrations of half-maximal velocity for sigmoidal and Michaelis–Menten models, respectively, and K_i is the inhibition constant. For experiments where the concentration of BFC was varied, 5 μM AdoMet was used. For experiments where the concentration of AdoMet was varied, 4 μM BFC was used. To account for the background activity due to endogenous human ICMT in the HEK293 cell lysate, initial velocity curves were constructed using lysate from cells transfected with GFP alone and subtracted for all analyses. The effective BFC concentration was corrected for the small amount of BFC that binds to plasticware used in the assay as described[12].

FSEC and western analysis of ICMT using a cleavable M2–M3 linker. cDNA encoding beetle ICMT was cloned into the pNGFP-EU expression vector[26] using the EcoRI and SalI restriction sites to create an ICMT construct with a 6× His tag and GFP fused to the N terminus (His–GFP–ICMT). A PreScission protease (PS) cleavage site and several flanking amino acids were inserted into the loop between the M2 and M3 helices (introduced between Asn58 and Glu59 to yield the final sequence Asn58–SGSSGSLEVLFQGPSAGGSAGAAS–Glu59, where the underlined region is the PS site) using standard molecular biology techniques. These constructs, with or without the cleavage site, were expressed by transient transfection in HEK293 cells (~1.5×10^6 cells using Lipofectamine 2000, Invitrogen). HEK293 cells were obtained from ATCC and were not tested for mycoplasma contamination. The cells were pelleted (500*g*), 48 h after transfection and re-suspended in 300 μl of buffer consisting of 50 mM NaH_2PO_4, pH 7.5, 190 mM NaCl, 10 mM KCl, 20 mM DTT, 200 μM AdoHcy, 40 mM dodecyl maltoside (DDM, Anatrace) detergent and 1:500 dilution of Protease Inhibitor Cocktail Set III, EDTA-free (CalBiochem). Samples were rotated for 1 h at 4 °C to allow detergent extraction of ICMT from membranes, and then were centrifuged at 20,800*g* for 1 h at 4 °C. The supernatants, which contained detergent-solubilized ICMT, were divided into two portions. PreScission protease (2 μg; made in-house, but available from GE Healthcare) was added to one portion. The samples were incubated for 2 h at 4 °C and analysed by anti-His western blot (Anti-His_6 antibody, Roche Cat. # 04905318001) and by FSEC[26], using a Superose 6 column (GE Healthcare). The running buffer for FSEC was 20 mM NaH_2PO_4, pH 7.5, 190 mM NaCl, 10 mM KCl, 5 mM DTT and 1 mM DDM.

Data availability. Atomic coordinates and structure factors have been deposited in the Protein Data Bank (PDB) with accession numbers 5V7P (ICMT–monobody) and 5VG9 (ICMT alone).

25. Kawate, T. & Gouaux, E. Fluorescence-detection size-exclusion chromatography for precrystallization screening of integral membrane proteins. *Structure* **14,** 673–681 (2006).
26. Kilmartin, J. V., Wright, B. & Milstein, C. Rat monoclonal antitubulin antibodies derived by using a new nonsecreting rat cell line. *J. Cell Biol.* **93,** 576–582 (1982).
27. Long, S. B., Campbell, E. B. & Mackinnon, R. Crystal structure of a mammalian voltage-dependent Shaker family K^+ channel. *Science* **309,** 897–903 (2005).
28. Koide, S., Koide, A. & Lipovšek, D. Target-binding proteins based on the 10th human fibronectin type III domain (^{10}Fn3). *Methods Enzymol.* **503,** 135–156 (2012).
29. Koide, A. *et al.* Accelerating phage-display library selection by reversible and site-specific biotinylation. *Protein Eng. Des. Sel.* **22,** 685–690 (2009).
30. Stockbridge, R. B., Koide, A., Miller, C. & Koide, S. Proof of dual-topology architecture of Fluc F^- channels with monobody blockers. *Nat. Commun.* **5,** 5120 (2014).
31. Sha, F. *et al.* Dissection of the BCR-ABL signaling network using highly specific monobody inhibitors to the SHP2 SH2 domains. *Proc. Natl Acad. Sci. USA* **110,** 14924–14929 (2013).
32. Minor, W., Cymborowski, M., Otwinowski, Z. & Chruszcz, M. HKL-3000: the integration of data reduction and structure solution—from diffraction images to an initial model in minutes. *Acta Crystallogr. D* **62,** 859–866 (2006).
33. Bricogne, G., Vonrhein, C., Flensburg, C., Schiltz, M. & Paciorek, W. Generation, representation and flow of phase information in structure determination: recent developments in and around SHARP 2.0. *Acta Crystallogr. D* **59,** 2023–2030 (2003).
34. McCoy, A. J. *et al.* Phaser crystallographic software. *J. Appl. Crystallogr. D* **40,** 658–674 (2007).
35. Brunger, A. T. Version 1.2 of the crystallography and NMR system. *Nat. Protoc.* **2,** 2728–2733 (2007).
36. Adams, P. D. *et al.* PHENIX: a comprehensive Python-based system for macromolecular structure solution. *Acta Crystallogr. D* **66,** 213–221 (2010).
37. Emsley, P., Lohkamp, B., Scott, W. G. & Cowtan, K. Features and development of Coot. *Acta Crystallogr. D* **66,** 486–501 (2010).
38. Chen, V. B. *et al.* MolProbity: all-atom structure validation for macromolecular crystallography. *Acta Crystallogr. D* **66,** 12–21 (2010).
39. Strong, M. *et al.* Toward the structural genomics of complexes: crystal structure of a PE/PPE protein complex from *Mycobacterium tuberculosis*. *Proc. Natl Acad. Sci. USA* **103,** 8060–8065 (2006).
40. Griggs, A. M., Hahne, K. & Hrycyna, C. A. Functional oligomerization of the *Saccharomyces cerevisiae* isoprenylcysteine carboxyl methyltransferase, Ste14p. *J. Biol. Chem.* **285,** 13380–13387 (2010).
41. Dharmaiah, S. *et al.* Structural basis of recognition of farnesylated and methylated KRAS4B by PDEδ. *Proc. Natl Acad. Sci. USA* **113,** E6766–E6775 (2016).
42. Karplus, P. A. & Diederichs, K. Linking crystallographic model and data quality. *Science* **336,** 1030–1033 (2012).

© 2018 Macmillan Publishers Limited, part of Springer Nature. All rights reserved.

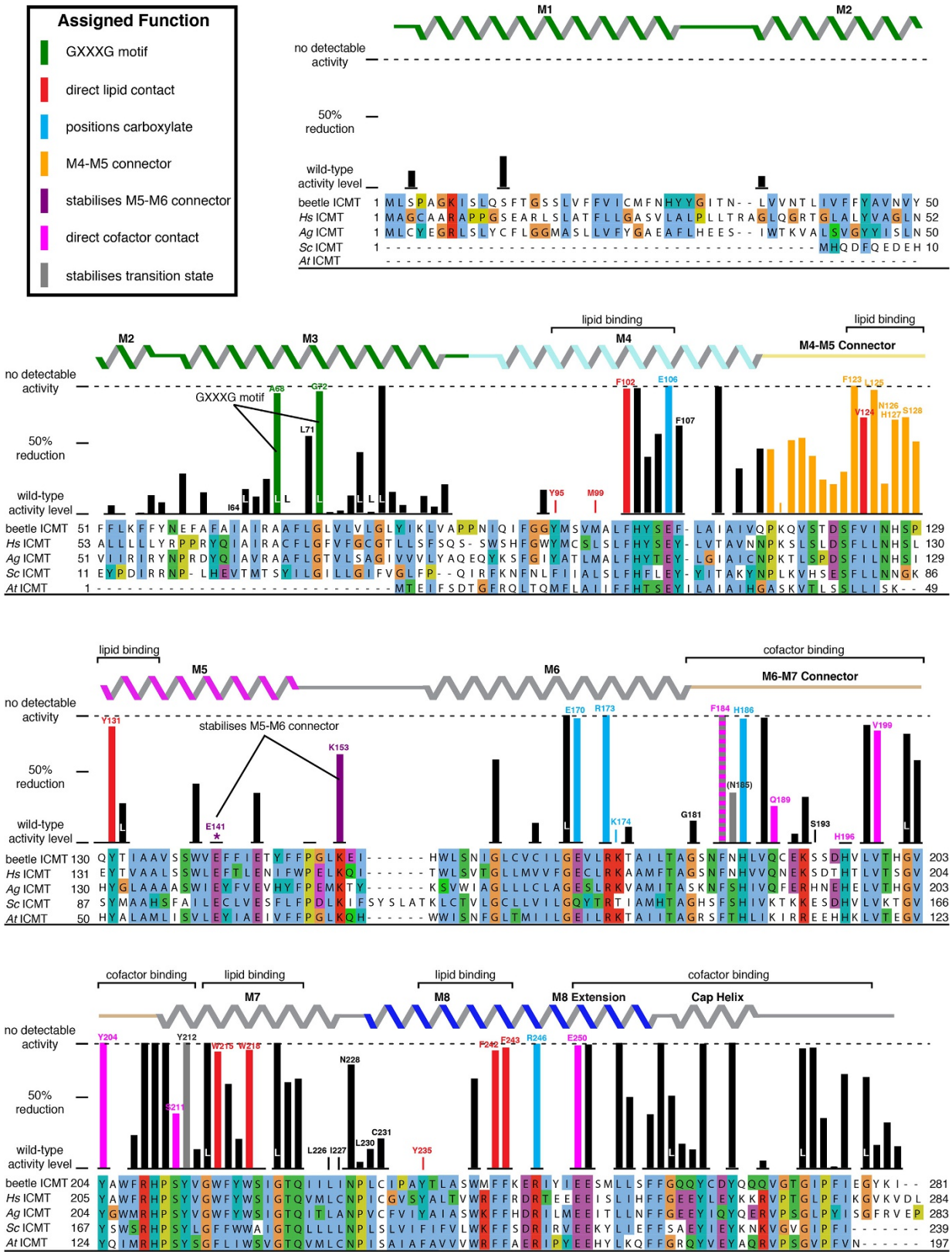

Extended Data Figure 1 | See next page for caption.

© 2018 Macmillan Publishers Limited, part of Springer Nature. All rights reserved.

Extended Data Figure 1 | The structure identifies functions for key residues. ICMT is displayed as a progression from primary sequence alignment, to the effects of scanning mutagenesis (bar graphs), to observed secondary structure (α-helices depicted as ribbons), to the assigned role of amino acids. Results from scanning mutagenesis experiments[12] are plotted above the sequence alignment as a bar graph showing the reduction of specific activity in comparison to wild-type ICMT, with 0% representing wild-type activity and 100% reflecting no detectable activity (indicated by a horizontal dashed line). The inset key denotes the colouring of the bar graph according to the functional role of the amino acid inferred from the atomic structure. Labelled brackets above the secondary structure denote the general function of the indicated regions of the primary sequence. In the bar graph: magenta, amino acids that contact AdoHcy; red, amino acids that line the lipid-binding cavity; blue, arginine residues that are proposed to form hydrogen bonds with the carboxylate of the prenylcysteine substrate, and the residues that position them; grey, residues proposed to form hydrogen bonds to the methyl of AdoHcy in the transition state; hydrogen bonds made with backbone atoms are indicated by parentheses surrounding the amino acid label. The mutagenesis data are derived from experiments using *A. gambiae* ICMT[12], and are normalized for expression level. Except where noted, the mutations were alanine substitutions. In some cases, leucine substitutions (L) were made (for example, when the wild-type amino acid was a glycine or alanine). The data represent triplicate measurements for each mutation and the mean s.d. is 11%. Gaps in the bar graph indicate amino acid positions that were not analysed by mutagenesis. Based on size-exclusion chromatography that was performed for each of the mutants, only the E141A mutation was found to be notably destabilizing (asterisk). A few mutations increased the activity relative to wild-type; these are shown as exhibiting 0% reduction in activity. The amino acid sequences included in the alignment are: *T. castaneum* ICMT (beetle ICMT), human (*Hs*), *A. gambiae* (*Ag*), *Saccharomyces cerevisiae* (*Sc*), and *Arabidopsis thaliana* (*At*) (UniProt accession numbers: D6WJ77, O60725, Q7PXA7, P32584 and Q93W54, respectively). The alignment is coloured according to the ClustalW convention.

© 2018 Macmillan Publishers Limited, part of Springer Nature. All rights reserved.

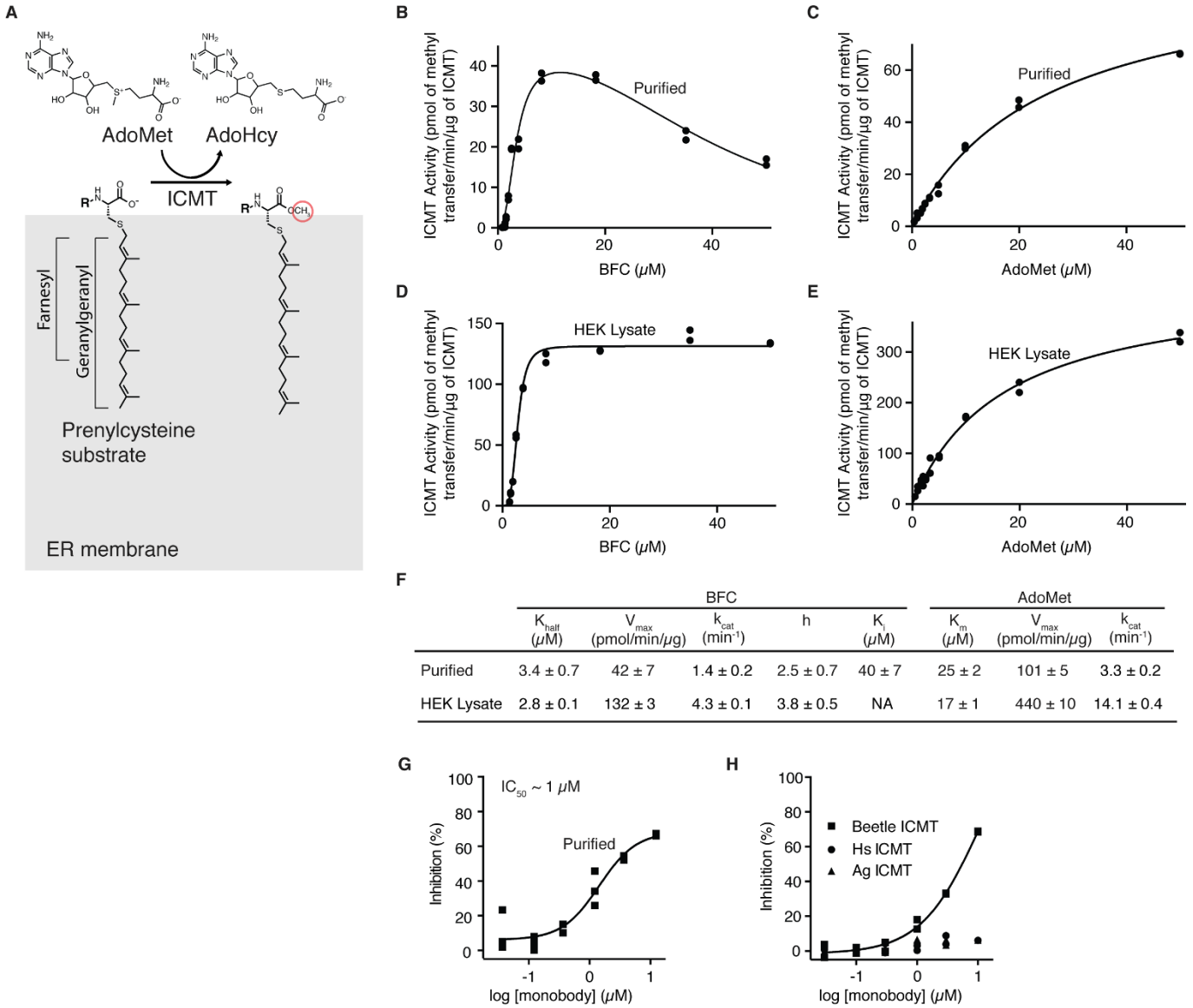

F

	BFC					AdoMet		
	K_{half} (µM)	V_{max} (pmol/min/µg)	k_{cat} (min^{-1})	h	K_i (µM)	K_m (µM)	V_{max} (pmol/min/µg)	k_{cat} (min^{-1})
Purified	3.4 ± 0.7	42 ± 7	1.4 ± 0.2	2.5 ± 0.7	40 ± 7	25 ± 2	101 ± 5	3.3 ± 0.2
HEK Lysate	2.8 ± 0.1	132 ± 3	4.3 ± 0.1	3.8 ± 0.5	NA	17 ± 1	440 ± 10	14.1 ± 0.4

Extended Data Figure 2 | Enzymatic activity and monobody inhibition of beetle ICMT. a, Schematic of the ICMT reaction. The shaded region represents the endoplasmic reticulum membrane; R, the protein portion of the substrate. In the minimal substrate AGGC, R is an acetyl group. For BFC, R is a biotin group. **b**–**e**, Activity of beetle ICMT, purified in DMNG detergent (**b**, **c**) or in cell lysate (**d**, **e**), shown as a plot of the formation of BFC-[^{3}H]methyl ester as a function of BFC concentration (**b, d**) or AdoMet concentration (**c, e**). For assays using HEK293 cells (**d**, **e**), ICMT was expressed as a fusion protein with GFP in order to quantify the amount of enzyme in the cell lysate (Methods). **f**, Kinetic parameters determined from the curves in **b**–**e**. Best-fit values (calculated in GraphPad Prism 7) are reported with the standard error of the fit. We observed a degree of substrate inhibition at higher concentrations of BFC (K_i ~40 µM) when using ICMT in detergent (**b**, **f**), which may be due to the dispersive nature of BFC when it exceeds the detergent concentration (10 µM). **g**, Dose–response curve showing the inhibitory effects of the monobody on the activity of purified beetle ICMT in detergent. **h**, Comparison of the effects of the monobody on the activities of beetle, human, and *A. gambiae* ICMT in HEK293 cell lysates. GFP–ICMT fusion proteins were used for the three orthologues and the concentration of each enzyme was determined using the fluorescence of GFP (Methods). The monobody inhibited beetle ICMT with an IC_{50} of ~7 µM in this assay, whereas no detectable inhibition of human or *A. gambiae* ICMT was observed. Individual data points are shown on the graphs (**b**–**e**, **g**, **h**).

© 2018 Macmillan Publishers Limited, part of Springer Nature. All rights reserved.

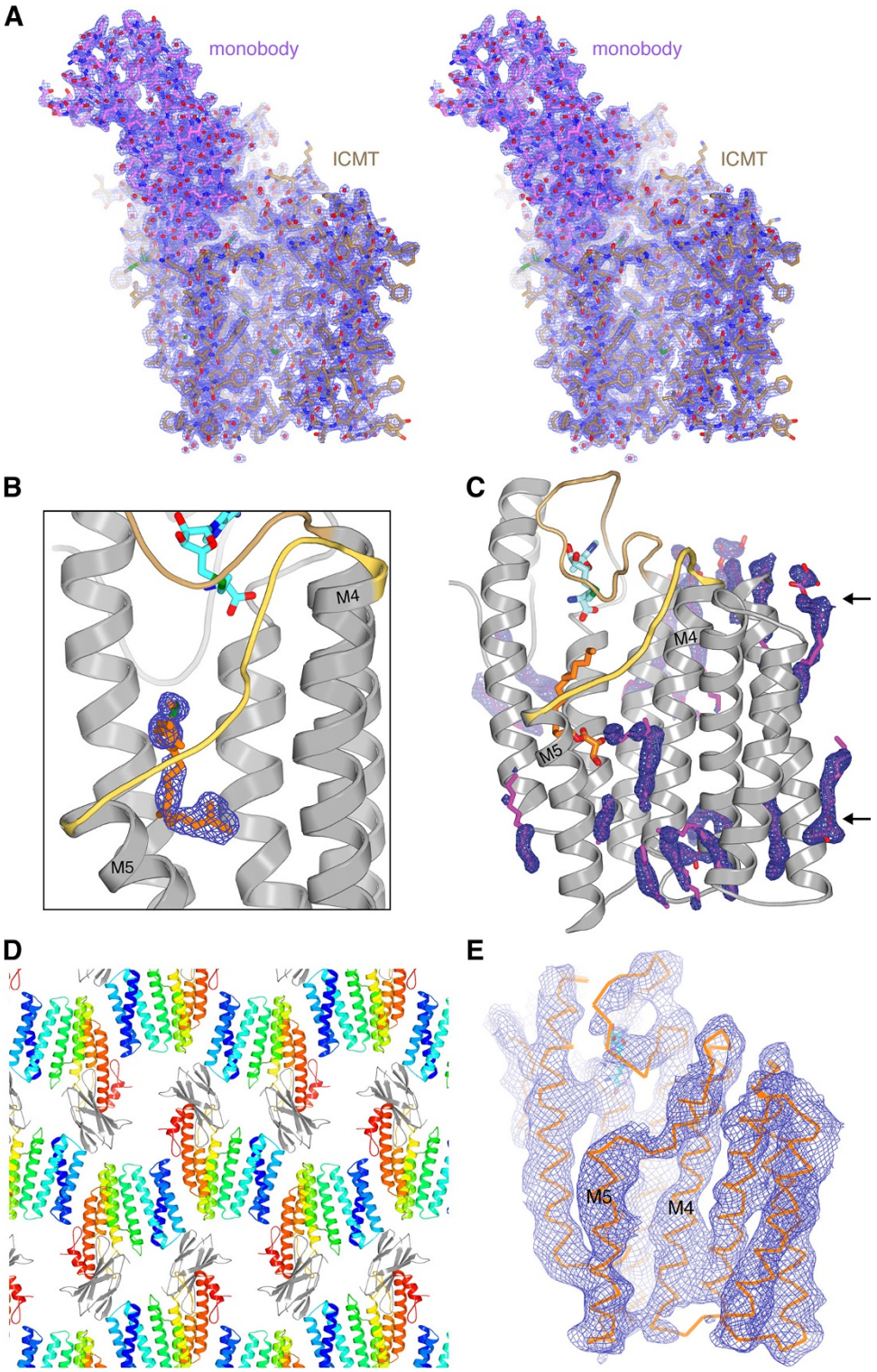

Extended Data Figure 3 | Electron density maps and crystal lattice. **a**, Stereo representation of the electron density for the ICMT–monobody complex (blue mesh, $2F_o$–F_c, countoured at 1.1σ, calculated from 35 to 2.3 Å resolution) drawn around the atomic model (stick representation). The monobody is coloured magenta; ICMT is tan. **b**, Electron density for the lipid in the active site from a composite simulated-annealing omit-electron density map ($2F_o$–F_c, contoured at 1σ and calculated from 35 to 2.3 Å resolution). The density would accommodate a geranylgeranyl lipid (orange sticks), as shown here. **c**, Electron density (blue mesh; $2F_o$–F_c map contoured at 1σ) for ordered monoolein lipids (magenta sticks) around ICMT. Monoolein lipids surround the transmembrane region of ICMT and collectively resemble a bilayer with typical thickness (arrows). The positioning of monoolein lipids in the vicinity of the M4–M5 connector (yellow) is consistent with the hypothesis that the enzyme would cause a slight depression in the membrane in this region, as illustrated in Extended Data Fig. 9. **d**, Crystal lattice in the ICMT–monobody complex, with ICMT coloured and the monobody in grey. **e**, A composite omit-electron-density map ($2F_o$–F_c, contoured at 1σ and calculated from 35 to 4.0 Å resolution) for the X-ray structure of ICMT without the monobody. The composite omit maps, which reduce model bias, were obtained using Phenix[36].

© 2018 Macmillan Publishers Limited, part of Springer Nature. All rights reserved.

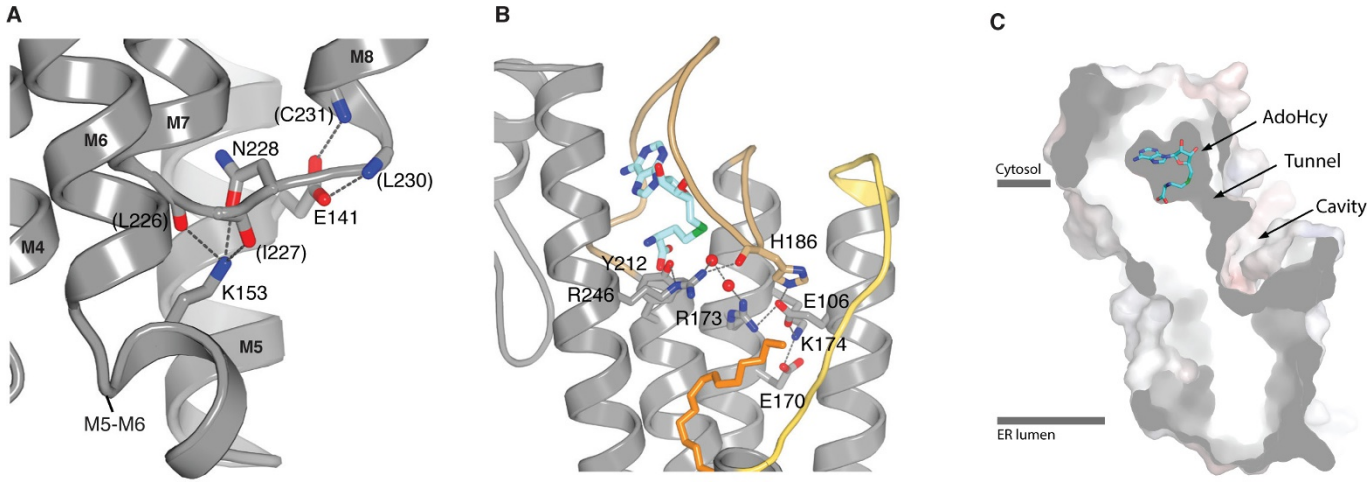

Extended Data Figure 4 | Interactions with the M5–M6 connector, interactions with active site arginine residues and cross-section of the active site. a, Interactions between the M5–M6 and M7–M8 connectors. The side chains of Glu141 (on M5) and Lys153 (on the M5–M6 connector) form hydrogen bonds (dashed lines) that cap the C-terminal end of M7 and the N-terminal end of M8, respectively. Portions of the amino acids involved are drawn as sticks. Parentheses indicate hydrogen bonds made with backbone atoms. Grey, carbon; blue, nitrogen; red, oxygen. **b**, Hydrogen-bonding network involving Arg173 and Arg246. Bonds (dashed lines) are made with surrounding amino acids (labelled sticks) and two water molecules (red spheres) in the active site. **c**, Cutaway view of the molecular surface of ICMT (grey), showing labelled regions of the active site. The view is approximately orthogonal to that shown in Fig. 2a. AdoHcy is drawn as sticks; approximate boundaries of the membrane are indicated by horizontal bars.

© 2018 Macmillan Publishers Limited, part of Springer Nature. All rights reserved.

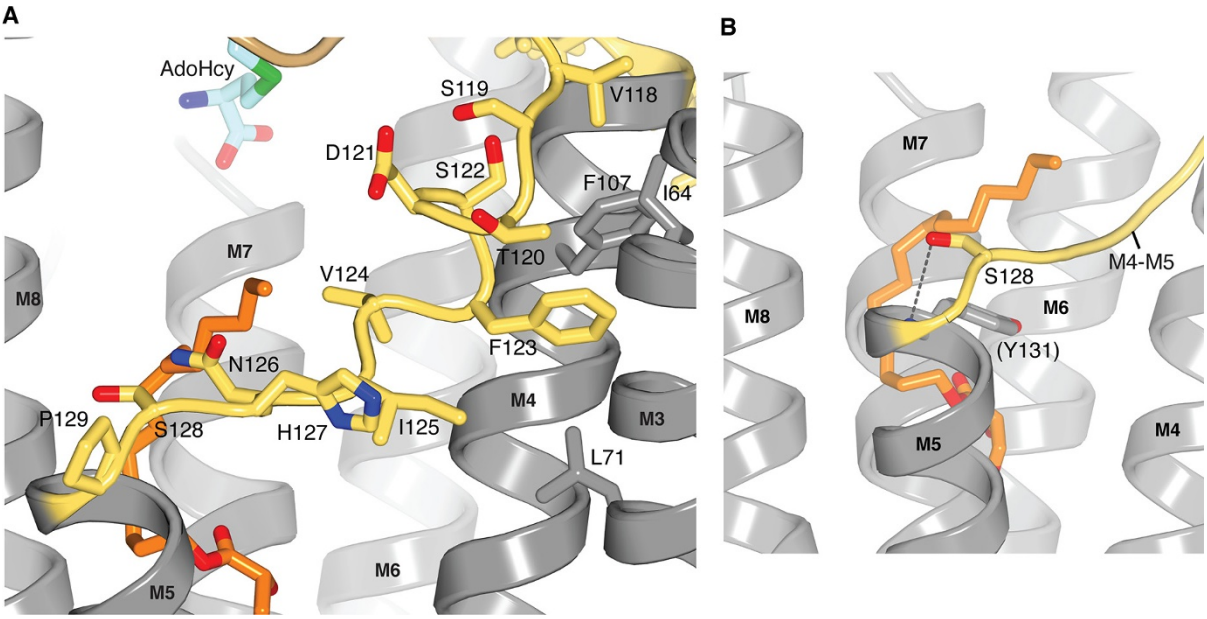

Extended Data Figure 5 | The M4–M5 connector. a, Close up view of the M4–M5 connector with side chains depicted as sticks. ICMT is predominately grey, with the M4–M5 connector coloured yellow. Amino acids that interact with Phe123 (Ile64, Leu71 and Phe107) are coloured grey. **b**, The N-terminal end of the M5 helix is capped by Ser128. The side chain of Ser128 is shown in stick representation, with the hydrogen bond to the backbone nitrogen atom of Tyr131 indicated by a dotted line.

© 2018 Macmillan Publishers Limited, part of Springer Nature. All rights reserved.

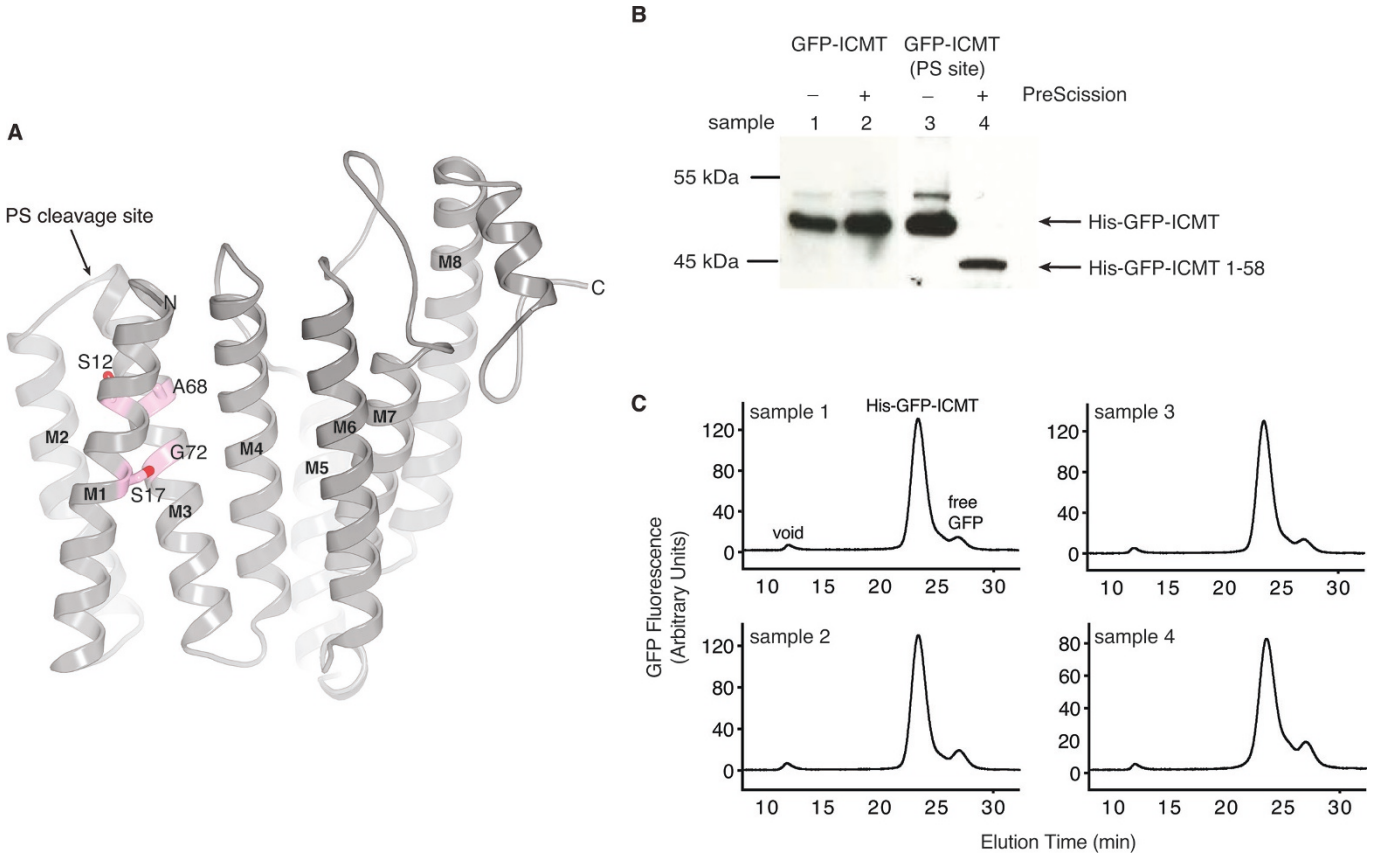

Extended Data Figure 6 | The M1–M2 portion of ICMT is an integral part of the enzyme. a, The GXXXG packing motif between helices M1 and M3 of ICMT. Residues on M1 and M3 that make contacts between these helices are drawn as sticks and coloured magenta. Because the M1 and M2 helices are not present in *S. cerevisiae* ICMT, we hypothesize that the GXXXG motif in the first transmembrane helix of yeast ICMT (equivalent to M3 of beetle ICMT) may cause dimerization of the yeast enzyme through packing of these helices[40], whereas ICMT enzymes that contain M1 and M2, which include human and beetle ICMT, are monomeric. The location of a PreScission protease cleavage site (PS site) that was introduced at Asn58, in the connection between the M2 and M3 helices, for experiments outlined in this figure, is indicated. **b**, Anti-His western blot showing that this cleavage site can be cleaved by PreScission protease. In this experiment, ICMT was expressed in HEK293 cells with an N-terminal His–GFP tag (His–GFP–ICMT), with or without the cleavage site. The addition of PreScission protease to detergent-solubilized sample 4 (His–GFP–ICMT with the cleavage site), but not control samples 1–3, results in a cleavage product consisting of His–GFP followed by amino acids 1–58 of ICMT (His–GFP–ICMT 1–58), which is detected by anti-His western blot. This confirms that the loop connecting the M2 and M3 helices is cut by the protease. Samples 1–3 are control experiments, as indicated. For gel source data, see Supplementary Fig. 1. **c**, FSEC profiles of the samples evaluated by western blot in **b** and numbered accordingly. Elution volumes for the void, His–GFP–ICMT and free GFP are indicated on the plot for sample 1. The cleavage of the M2–M3 loop by PreScission protease does not alter the elution profile (sample 4) in comparison to the other samples, which indicates that the cleaved portion (His–GFP–ICMT 1–58) is associated with the remainder of the enzyme via non-covalent interactions. No replicates of these experiments were performed.

© 2018 Macmillan Publishers Limited, part of Springer Nature. All rights reserved.

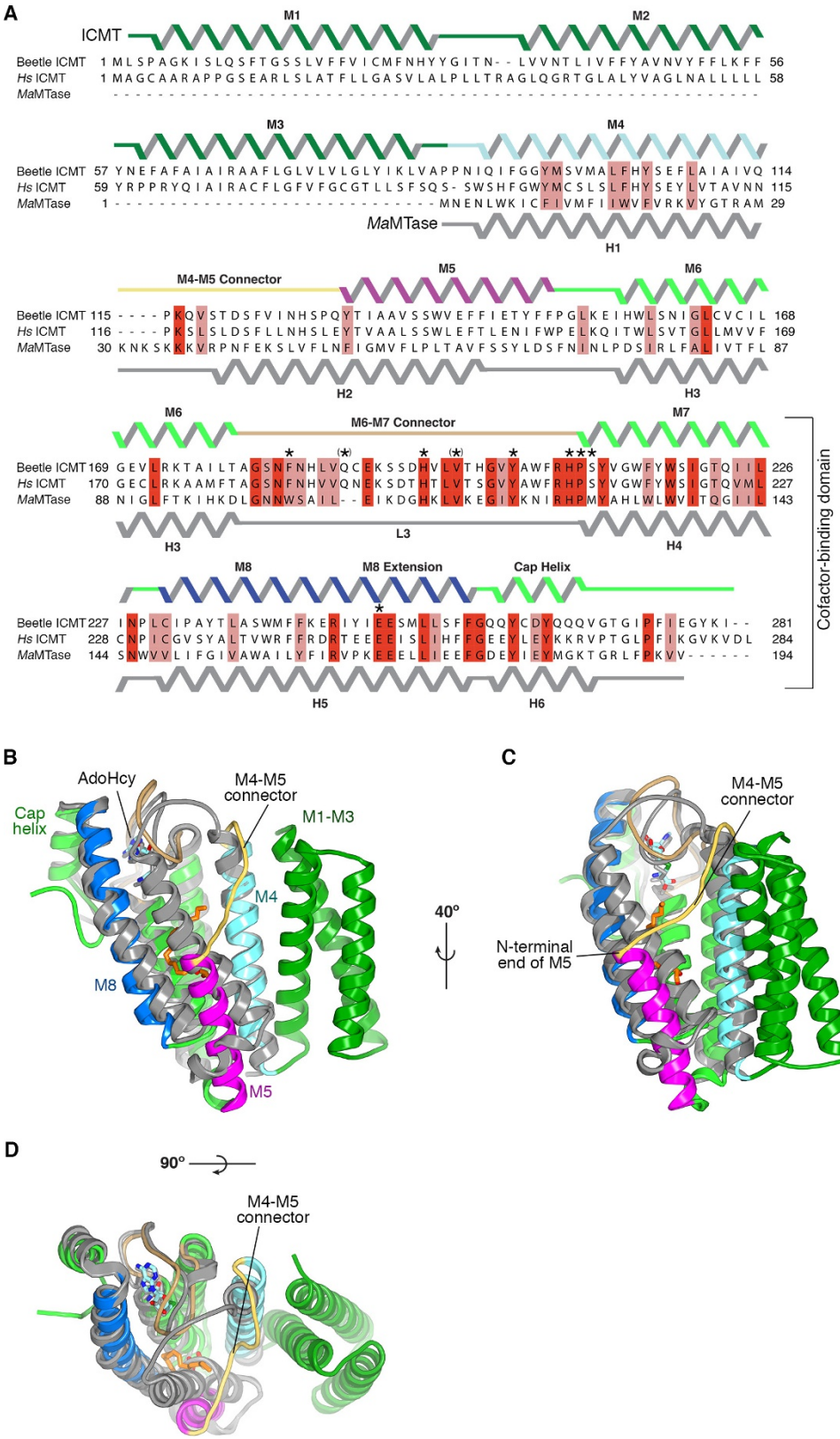

Extended Data Figure 7 | Comparison of ICMT and *Ma*MTase. **a**, Sequence alignment between beetle ICMT, human ICMT, and *Ma*MTase (referred to as *Ma*-ICMT in ref. 16). In the alignment, red colouring indicates identical residues and pink indicates similar residues. The secondary structures of ICMT and *Ma*MTase (PDB ID: 4A2N) are shown above and below the alignment, respectively. The region of highest sequence conservation corresponds to the cofactor-binding domain (bracketed); elsewhere there is low sequence similarity. Asterisks indicate amino acids of ICMT that contact AdoHcy; surrounding parentheses, where present, indicate that hydrogen bonds are made with backbone atoms. **b**–**d**, Superposition of the structures of beetle ICMT and *Ma*MTase, shown from three vantage points in cartoon representations. ICMT is coloured according to the colouring of its secondary structure in **a**; *Ma*MTase is coloured grey.

© 2018 Macmillan Publishers Limited, part of Springer Nature. All rights reserved.

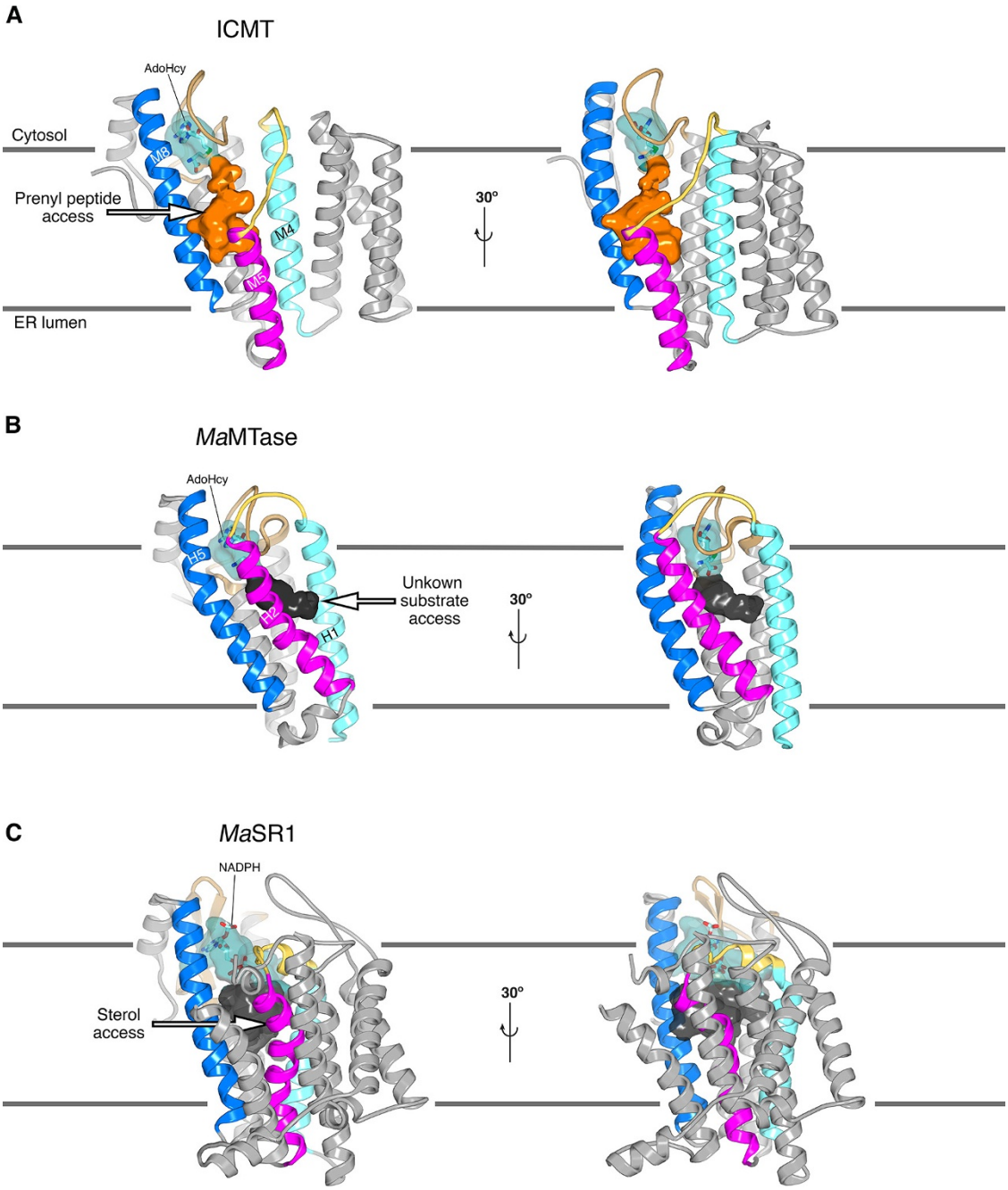

Extended Data Figure 8 | Comparison of the active sites of ICMT, *Ma*MTase and *Ma*SR1. a, Two orientations of the overall structure of ICMT are shown with the active site depicted as a molecular surface. The portion that binds AdoHcy is coloured cyan and is partially transparent to reveal a stick representation of the cofactor. The cavity that would be exposed to the membrane and forms the presumed binding site of the prenylcysteine moiety of the substrate is coloured orange. An arrow marks a pathway by which the prenyl group of the substrate could reach the active site via the membrane. Horizontal lines denote the approximate boundaries of the endoplasmic reticulum membrane. **b**, Overall structure of *Ma*MTase (PDB ID: 4A2N) shown in two orientations, obtained by superposing with ICMT. A cavity, denoting the active site, is drawn as a molecular surface. The portion in which AdoHcy binds is coloured cyan; the remainder is dark grey and is likely to represent the binding site of its biological substrates, which are unknown. Structural elements are coloured as for ICMT in **a**. The cavity is exposed to the membrane on the opposite side of the enzyme relative to ICMT. Instead of a crevice between the magenta- and dark-blue-coloured helices like ICMT (H2 and H5 of *Ma*MTase, which roughly correspond to M5 and M8 of ICMT, respectively), *Ma*MTase has a crevice between H1 (light blue) and H2 (magenta), suggesting that its substrates access it from the 'right' (arrow) rather than from the 'left'. In ICMT, this route is blocked by the M4–M5 linker. The dimensions of the cavity in *Ma*MTase and its exposure to the membrane suggest that the substrates of *Ma*MTase are hydrophobic molecules that are smaller than a farnesyl or geranylgeranyl prenyl group. **c**, Overall structure of the prokaryotic integral membrane sterol reductase *Ma*SR1 (PDB ID: 4QUV)[18]. The orientation is based on superposition of the cofactor-binding domain with ICMT, with corresponding colouring. The carbon atoms of a bound NADPH cofactor are coloured cyan. A crevice between the magenta and dark blue-coloured helices may serve as access for lipophilic sterol substrates[18] (arrow).

© 2018 Macmillan Publishers Limited, part of Springer Nature. All rights reserved.

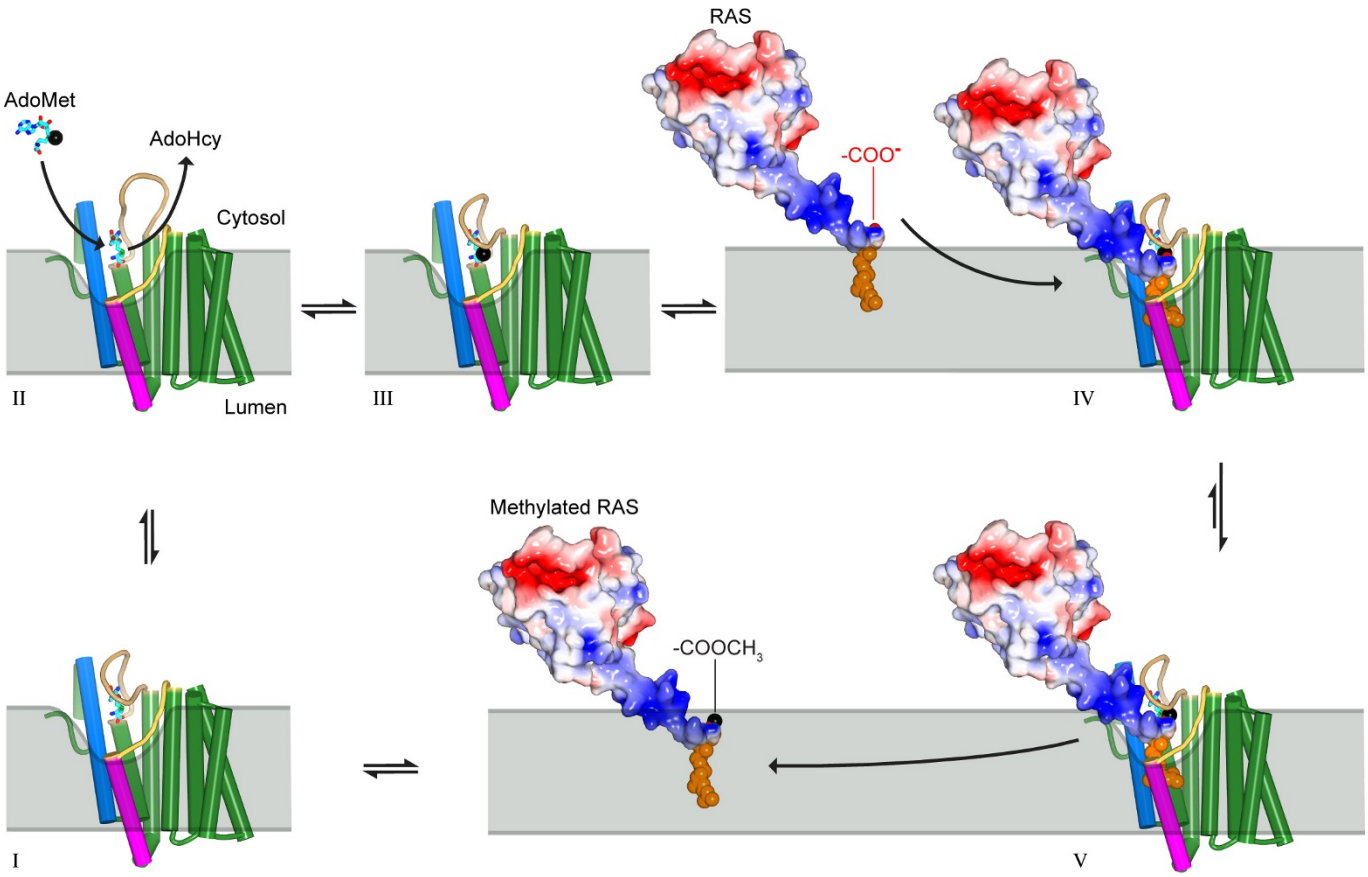

Extended Data Figure 9 | Proposed reaction cycle for ICMT. Major steps along the reaction coordinate (I–V). From the AdoHcy-bound state (I), a hinged displacement of the M6–M7 connector loop (II) allows release of AdoHcy and exchange for AdoMet from the cytosol (III). The C-terminal prenyl group of the substrate is located within the endoplasmic reticulum membrane before methylation, as depicted for KRAS4B in the figure, and approaches the enzyme by 2D diffusion within the membrane. The prenylcysteine reaches the active site by passing between the M5 and M8 helices (coloured magenta and blue, respectively). In the ternary complex (IV), substrate–enzyme contacts are limited to interactions with the prenyl group and the C-terminal carboxylate, giving rise to specificity for these elements within the context of a wide range of protein substrates. A cytosolic cleft above the M5–M8 crevice that leads to the active site accommodates the polar C-terminal peptide of protein substrates (for example, the polybasic region of KRAS4B, coloured blue). The inhibitory monobody occupies this region. Catalysis proceeds from the ternary complex, and the product, made more lipophilic by methylation and neutralization of a negative charge, is able to diffuse into the membrane (V). ICMT is shown as a cartoon with helices drawn as cylinders and the AdoHcy or AdoMet cofactors depicted as cyan sticks. A black sphere indicates the methyl group of AdoMet. Prenylated KRAS4B (based on PDB ID: 5TAR[41]) is depicted as a molecular surface and coloured according to electrostatic potential (red, negative; blue, positive) with its prenyl group shown as orange spheres. The endoplasmic reticulum membrane is depicted in grey and curved in the vicinity of the active site to suggest that the enzyme might modulate the local distribution of lipid molecules to facilitate substrate access.

© 2018 Macmillan Publishers Limited, part of Springer Nature. All rights reserved.

Extended Data Table 1 | Data collection, phasing and refinement statistics

	ICMT-monobody Native	ICMT-monobody SeMet	ICMT Native
Data Collection	APS 24-ID-C	APS 23-ID-D	APS 23-ID-D
Space group	$P2_12_12_1$	$P2_12_12_1$	$C222_1$
Wavelength (Å)	0.9790	0.9791	1.0332
Cell dimensions:			
a, b, c (Å)	40.6, 87.7, 147.7	40.8, 88.7, 148.4	51.6, 123.6, 236.1
α, β, γ (°)	90, 90, 90	90, 90, 90	90, 90, 90
Resolution (Å)	31 - 2.3 (2.34 - 2.3)	40 - 3.0 (3.05 - 3.0)	33 - 4.0 (4.07 - 4.0)
No. of crystals	1	9	1
R_{merge} (%)	20.6 (97.9)	64.2 (>100.0)	7.1 (>100.0)
R_{pim} (%)	6.2 (29.5)	9.6 (57.0)	1.2 (34.0)
I/σI	13.3 (2.5)	15.5 (2.0)	85 (3.0)
Completeness (%)	97.2 (99.8)	100.0 (100.0)	100.0 (100.0)
Redundancy	11.2 (11.1)	45.7 (47.9)	34.6 (35.6)
SIRAS Phasing		30 – 4.0 Å	
No. of sites		5	
Phasing Power (iso / ano)		0.129 / 0.292	
R_{cullis} (iso / ano) (%)		95.5 / 97.5	
Figure of Merit (acentric / centric)		0.183 / 0.047	
Refinement			
Resolution (Å)	31 - 2.3 (2.4 - 2.3)		33 - 4.0 (5.0 - 4.0)
No. of reflections	23,203		6,119
R_{work} (%)	21.4 (26.9)		36.9 (45.0)
R_{free} (%)	24.6 (32.2)		38.9 (42.2)
No. atoms			
Protein	3039		2250
Ligands	319		26
Water	92		
Average B-factors (Å^2)			
Protein	33.4		209.6
Ligands	58.6		200.7
Water	38.7		
Ramachandran (%)			
Favoured	98.1		97.3
Outliers	0.0		0.0
R.m.s. deviations			
Bond lengths (Å)	0.003		0.004
Bond angles (°)	0.595		0.745
Clash Score	2.3		24

Data collection statistics are from HKL3000 (ref. 32); phasing statistics are from SHARP[33]; refinement statistics are from PHENIX[36]. CC1/2 is defined in ref. 42; Clash Score is defined in ref. 38. $R_{sym} = \Sigma |I_i - \langle I_i \rangle| / \Sigma I_i$, where $\langle I_i \rangle$ is the average intensity of symmetry-equivalent reflections. Phasing power = r.m.s. ($|F|/\varepsilon$), where $|F|$ is the heavy-atom structure-factor amplitude and ε is the residual lack of closure error (r.m.s. is root mean square). R_{cullis} is the mean-residual lack-of-closure error divided by the dispersive or anomalous difference. R-factor $= \Sigma |F_o - F_c| / \Sigma |F_o|$, where F_o and F_c are the observed and calculated structure factors, respectively. R_{free} = R-factor calculated using a subset (~5%) of reflection data chosen randomly and omitted throughout refinement. Numbers in parentheses indicate the highest-resolution shells and their statistics.

© 2018 Macmillan Publishers Limited, part of Springer Nature. All rights reserved.

nature research

Corresponding author(s): Stephen B. Long

☐ Initial submission ☐ Revised version ☒ Final submission

Life Sciences Reporting Summary

Nature Research wishes to improve the reproducibility of the work that we publish. This form is intended for publication with all accepted life science papers and provides structure for consistency and transparency in reporting. Every life science submission will use this form; some list items might not apply to an individual manuscript, but all fields must be completed for clarity.

For further information on the points included in this form, see Reporting Life Sciences Research. For further information on Nature Research policies, including our data availability policy, see Authors & Referees and the Editorial Policy Checklist.

Experimental design

1. Sample size

Describe how sample size was determined.

Highly redundant diffraction data were used for structure determination and refinement of the atomic model (Extended Data Table 1).

2. Data exclusions

Describe any data exclusions.

No data were excluded from the analyses.

3. Replication

Describe whether the experimental findings were reliably reproduced.

All attempts at replication were successful. Crystals consistently grew under the indicated conditions and diffracted to similar resolution.

4. Randomization

Describe how samples/organisms/participants were allocated into experimental groups.

As is standard practice in X-ray crystallography, a random set of structure factors were held aside during the refinement and were used to calculate R(free), as indicated in the Methods and Extended Data Table 1.

5. Blinding

Describe whether the investigators were blinded to group allocation during data collection and/or analysis.

The investigators were blinded to the randomly selected set of structure factors that were used to calculate R(free).

Note: all studies involving animals and/or human research participants must disclose whether blinding and randomization were used.

6. Statistical parameters

For all figures and tables that use statistical methods, confirm that the following items are present in relevant figure legends (or in the Methods section if additional space is needed).

n/a	Confirmed	
☐	☒	The exact sample size (*n*) for each experimental group/condition, given as a discrete number and unit of measurement (animals, litters, cultures, etc.)
☐	☒	A description of how samples were collected, noting whether measurements were taken from distinct samples or whether the same sample was measured repeatedly
☐	☒	A statement indicating how many times each experiment was replicated
☒	☐	The statistical test(s) used and whether they are one- or two-sided (note: only common tests should be described solely by name; more complex techniques should be described in the Methods section)
☒	☐	A description of any assumptions or corrections, such as an adjustment for multiple comparisons
☒	☐	The test results (e.g. *P* values) given as exact values whenever possible and with confidence intervals noted
☐	☒	A clear description of statistics including central tendency (e.g. median, mean) and variation (e.g. standard deviation, interquartile range)
☒	☐	Clearly defined error bars

See the web collection on statistics for biologists for further resources and guidance.

Software

Policy information about availability of computer code

7. Software

Describe the software used to analyze the data in this study.	All software used is indicated in the Methods, and consists of published, publicly available, software used routinely for X-ray crystallography. This includes: Phenix, coot, pymol, and CNS.

For manuscripts utilizing custom algorithms or software that are central to the paper but not yet described in the published literature, software must be made available to editors and reviewers upon request. We strongly encourage code deposition in a community repository (e.g. GitHub). *Nature Methods* guidance for providing algorithms and software for publication provides further information on this topic.

Materials and reagents

Policy information about availability of materials

8. Materials availability

Indicate whether there are restrictions on availability of unique materials or if these materials are only available for distribution by a for-profit company.	There are no restrictions on availability of unique materials.

9. Antibodies

Describe the antibodies used and how they were validated for use in the system under study (i.e. assay and species).	Anti-HIS6 antibody, Roche Cat# 04905318001

10. Eukaryotic cell lines

a. State the source of each eukaryotic cell line used.	Pichia pastoris strain SMD1168, from Invitrogen. HEK-293 cells from ATCC
b. Describe the method of cell line authentication used.	N/A
c. Report whether the cell lines were tested for mycoplasma contamination.	Not tested.
d. If any of the cell lines used are listed in the database of commonly misidentified cell lines maintained by ICLAC, provide a scientific rationale for their use.	N/A

Animals and human research participants

Policy information about studies involving animals; when reporting animal research, follow the ARRIVE guidelines

11. Description of research animals

Provide details on animals and/or animal-derived materials used in the study.	No animals were used.

Policy information about studies involving human research participants

12. Description of human research participants

Describe the covariate-relevant population characteristics of the human research participants.	The study did not involve human research participants.